

An ultra-wideband 2-bit coding metasurface using Pancharatnam—Berry phase for radar cross-section reduction

Bao-Qin Lin(林宝勤), Wen-Zhun Huang(黄文准), Lin-Tao Lv(吕林涛), Jian-Xin Guo(郭建新),Yan-Wen Wang(王衍文), and Hong-Jun Ye(叶红军)

Citation: Chin. Phys. B, 2022, 31 (**3**): 034204. DOI: 10.1088/1674-1056/ac11ec
Journal homepage: http://cpb.iphy.ac.cn; http://iopscience.iop.org/cpb

What follows is a list of articles you may be interested in

A novel polarization converter based on the band-stop frequency selective surface

Kun Liao(廖昆), Shining Sun(孙世宁), Xinyuan Zheng(郑昕原), Xianxian Shao(邵纤纤), Xiangkun Kong(孔祥鲲), and Shaobin Liu(刘少斌)

Chin. Phys. B, 2022, 31 (**2**): 024211. DOI: 10.1088/1674-1056/ac1fdd

Efficient manipulation of terahertz waves by multi-bit coding metasurfaces and further applications of such metasurfaces

Yunping Qi(祁云平) Baohe Zhang(张宝和), Jinghui Ding(丁京徽), Ting Zhang(张婷), Xiangxian Wang(王向贤), and Zao Yi(易早)

Chin. Phys. B, 2021, 30 (**2**): 024211. DOI: 10.1088/1674-1056/abd6fc

Hyperbolic metamaterials for high-efficiency generation of circularly polarized Airy beams

Lin Chen(陈林), Huihui Li(李会会), Weiming Hao(郝玮鸣), Xiang Yin(殷祥), Jian Wang(王健)

Chin. Phys. B, 2020, 29 (**8**): 084210. DOI: 10.1088/1674-1056/ab96a1

Pancharatnam-Berry metasurface for terahertz wave radar cross section reduction

Shao-He Li(李绍和), Jiu-Sheng Li(李九生)

Chin. Phys. B, 2019, 28 (**9**): 094210. DOI: 10.1088/1674-1056/ab33f5

A method for generating double-ring-shaped vector beams

Huan Chen(陈欢), Xiao-Hui Ling(凌晓辉), Zhi-Hong Chen(陈知红), Qian-Guang Li(李钱光), Hao Lv(吕昊), Hua-Qing Yu(余华清), Xu-Nong Yi(易煦农)

Chin. Phys. B, 2016, 25 (**7**): 074201. DOI: 10.1088/1674-1056/25/7/074201

An ultra-wideband 2-bit coding metasurface using Pancharatnam–Berry phase for radar cross-section reduction

Bao-Qin Lin(林宝勤)[†], Wen-Zhun Huang(黄文准), Lin-Tao Lv(吕林涛), Jian-Xin Guo(郭建新), Yan-Wen Wang(王衍文), and Hong-Jun Ye(叶红军)

School of Information Engineering, Xijing University, Xi'an 710123, *China*

(Received 27 May 2021; revised manuscript received 28 June 2021; accepted manuscript online 7 July 2021)

An ultra-wideband 2-bit coding metasurface is designed for radar cross-section (RCS) reduction. The design process is presented in detail, in which a polarization conversion metasurface (PCM) is first proposed. The proposed PCM can realize ultra-wideband circular polarization (CP) maintaining reflection. Moreover, Pancharatnam–Berry (PB) phase will be generated in the co-polarized reflection coefficient by rotating the metallic patches in its unit cells. Thus, based on the PCM, the four coding elements of a 2-bit coding metasurface are constructed using PB phase, and an ultra-wideband PB 2-bit coding metasurface is proposed according to an appropriate coding sequence. The simulated and experimental results show that the coding metasurface has obvious advantages of wideband and polarization-insensitivity. Compared to a metallic plate of the same size, it can achieve more than 10 dB RCS reduction in the frequency band from 9.8 GHz to 42.6 GHz with a relative bandwidth of 125.2% under normal incidence with arbitrary polarizations.

Keywords: coding metasurface, Pancharatnam–Berry phase, radar cross-section (RCS)

PACS: 42.25.Ja, 42.79.Fm, 78.20.Ci **DOI:** 10.1088/1674-1056/ac11ec

1. Introduction

Metasurface is a kind of 2D planar metamaterial, which is an artificial composite surface composed of sub-wavelength resonant unit cell structures. Through the reasonable design of the unit cell structures, almost all the basic properties of electromagnetic (EM) waves can be tailored by using various metasurfaces. Due to the favorable characteristics of metasurfaces, a variety of metasurfaces, such as metasurface absorbers,[1–5] artificial magnetic conductors (AMC)[6–11] and coding metasurfaces[12–30] have been proposed to reduce the radar cross-section (RCS) of stealth targets.

The firs coding metasurface was proposed by Cui *et al.* in 2014,[12] which consisted of several different types of coding elements arranged at random. Because the reflection phases in various types of coding elements were very different, the coding metasurface could achieve broadband RCS reduction due to phase cancelation after optimizing the arrangement of these elements. In a coding metasurface, the type of coding elements can be represented as a binary digit according to their different phase responses. For example, for a 2-bit coding metasurface, the codes "00", "01", "10", and "11" can represent the coding elements with relative phase responses 0°, 90°, 180°, and 270°, respectively. Therefore, the array pattern of a coding metasurface can be represented by a coding sequence, and based on several proper coding elements, a desired coding metasurface can be proposed by optimizing the coding sequence. Based on the above, we know that the design procedure of a coding metasurface will mainly consist of the following two steps: one is to design several proper coding elements with suitable phase responses, and the other is to obtain an appropriate coding sequence. In recent years, to realize broadband RCS reduction, coding metasurface has attracted significant attention and many different designs have been proposed. The simplest case is 1-bit coding metasurface,[13–19] which consists of only two types of elements denoted as '0' and '1'. When the reflection phase difference between 0 and 1 elements can be maintained between $180 + 37$ in a specific frequency range, 10-dB RCS reduction will be realized in the band due to phase cancelation. In Refs. [20–23], a series of 2-bit coding metasurfaces have been presented. For a 2-bit coding metasurface composed of four types of elements with relative reflection phases 0°, 90°, 180°, and 270°, it can be seen as a combiner of two different 1-bit coding metasurfaces Thus, it can achieve greater freedom for controlling EM waves. When the four types of elements are arrayed according to an appropriate coding sequence, it displays better performance in RCS reduction.[12]

In this work, to design an ultra-wideband 2-bit coding metasurface for RCS reduction using Pancharatnam–Berry (PB) phase, a polarization conversion metasurface (PCM) is first proposed. The simulated results show that the PCM can make the magnitude of its co-polarized reflection coefficient under CP incidence close to 1.0 in the ultra-wide frequency range from 9.8 GHz to 43.3 GHz, and when the metallic patch in its unit cells is rotated by an angle ψ, almost $\pm 2\psi$ PB phase will be generated in the co-polarized reflection coeffi-

[†]Corresponding author. E-mail: aflbq@sina.com

© 2022 Chinese Physical Society and IOP Publishing Ltd

cient. Thus, based on the PCM, an ultra-wideband 2-bit PB coding metasurface is successfully proposed. The simulated and experimental results show that the coding metasurface can realize RCS reduction under arbitrary polarization incidences. Moreover, its working band (9.8 GHz to 42.6 GHz) is almost the same as that of the original PCM (9.8 GHz to 43.3 GHz).

2. Design and analysis of the coding elements

To design a reflective 2-bit coding metasurface, four coding elements with relative reflection phases of 0°, 90°, 180° and 270° need to be constructed. In this work, to construct the four appropriate coding elements using PB phase, an ultra-wideband PCM is first proposed, which consists of a metallic patch array printed on the top of a dual-layer grounded dielectric substrate. One of its unit cells is shown in Fig. 1. It can be seen that the metallic patch in the unit cell is a circular structure, which is most suitable for rotation to generate PB phase. Moreover, the metallic patch is an anisotropic structure with a pair of symmetric axes u and v, which are perpendicular to each other. We define the angle between the positive u-axis and positive x-axis as the rotation angle ψ of the metallic patch, now the metallic patch has been rotated by $\psi = 45°$. In addition, the geometrical parameters of the unit cell structure are shown in Fig. 1. After appropriate selection, the following geometrical parameters were chosen: $P = 6.00$ mm, $r = 2.60$ mm, $w = 0.20$ mm, $g = 1.40$ mm, $t = 0.20$ mm, $\alpha = 38°$, $h_1 = 0.50$ mm and $h_2 = 2.00$ mm. In addition, the metallic patch, together with the grounded plane, is modeled as a 0.017-mm copper film with electric conductivity $\sigma = 5.8 \times 10^7$ S/m. Moreover, the dual-layer dielectric substrate consists of a PTFE dielectric layer and foam layer, whose relative permittivities are $\varepsilon_{r1} = 1.80$ and $\varepsilon_{r2} = 1.05$, respectively.

Due to the symmetry of the PCM structure, in the uv-coordinate system, the reflection matrix $\boldsymbol{R}_{\text{lin-}uv}$ for a linearly polarized (LP) wave can be expressed as

$$\boldsymbol{R}_{\text{lin-}uv} = \begin{pmatrix} r_{uu} & 0 \\ 0 & r_{vv} \end{pmatrix}, \tag{1}$$

wherein the magnitude of r_{uu} and r_{vv} will both be very close to 1.0 because the dielectric loss is very small. Thus, the following formula can be established when the small dielectric loss is neglected:

$$r_{vv} = r_{uu} \mathrm{e}^{-\mathrm{j}\Delta\varphi_{uv}}, \tag{2}$$

wherein $\Delta\varphi_{uv}$ denotes the phase difference between r_{uu} and r_{vv}.

When the metallic patch in the unit cell of the PCM is rotated by ψ, as shown in Fig. 1(a), the electric field components in the uv-coordinate system can be converted to those in the xy-coordinate system using the following formula:

$$\begin{pmatrix} E_x \\ E_y \end{pmatrix} = \begin{pmatrix} \cos\psi & -\sin\psi \\ \sin\psi & \cos\psi \end{pmatrix} \begin{pmatrix} E_u \\ E_v \end{pmatrix}. \tag{3}$$

Thus, the reflection matrix $R_{\text{lin-}xy}$ in the xy-coordinate system can be obtained through the following formula derivation:

$$\begin{aligned} \begin{pmatrix} E_x^{\mathrm{r}} \\ E_y^{\mathrm{r}} \end{pmatrix} &= \begin{pmatrix} \cos\psi & -\sin\psi \\ \sin\psi & \cos\psi \end{pmatrix} \begin{pmatrix} E_u^{\mathrm{r}} \\ E_v^{\mathrm{r}} \end{pmatrix} = \begin{pmatrix} \cos\psi & -\sin\psi \\ \sin\psi & \cos\psi \end{pmatrix} \begin{pmatrix} r_{uu} & 0 \\ 0 & r_{vv} \end{pmatrix} \begin{pmatrix} E_u^{\mathrm{i}} \\ E_v^{\mathrm{i}} \end{pmatrix} \\ &= \begin{pmatrix} \cos\psi & -\sin\psi \\ \sin\psi & \cos\psi \end{pmatrix} \begin{pmatrix} r_{uu} & 0 \\ 0 & r_{vv} \end{pmatrix} \begin{pmatrix} \cos\psi & -\sin\psi \\ \sin\psi & \cos\psi \end{pmatrix}^{-1} \begin{pmatrix} E_x^{\mathrm{i}} \\ E_y^{\mathrm{i}} \end{pmatrix}, \end{aligned} \tag{4}$$

$$\begin{aligned} \boldsymbol{R}_{\text{Lin-}xy} &= \begin{pmatrix} \cos\psi & -\sin\psi \\ \sin\psi & \cos\psi \end{pmatrix} \begin{pmatrix} r_{uu} & 0 \\ 0 & r_{vv} \end{pmatrix} \begin{pmatrix} \cos\psi & -\sin\psi \\ \sin\psi & \cos\psi \end{pmatrix}^{-1} \\ &= \begin{pmatrix} r_{uu}\cos\psi & -r_{vv}\sin\psi \\ r_{uu}\sin\psi & r_{vv}\cos\psi \end{pmatrix} \begin{pmatrix} \cos\psi & \sin\psi \\ -\sin\psi & \cos\psi \end{pmatrix} \\ &= \begin{pmatrix} r_{uu}\cos^2\psi + r_{vv}\sin^2\psi & (r_{uu} - r_{vv})\cos\psi\sin\psi \\ (r_{uu} - r_{vv})\cos\psi\sin\psi & r_{uu}\sin^2\psi + r_{vv}\cos^2\psi \end{pmatrix}. \end{aligned} \tag{5}$$

When the proposed PCM is under CP normal incidence, since the CP incident wave is in $-z$ axis direction, the unit waves of the right-handed CP (RCP) incident and left-handed CP (LCP) reflected waves are both expressed as $\hat{e}_+^{\mathrm{i}} = \hat{e}_-^{\mathrm{r}} = \hat{e}_x + \mathrm{j}\hat{e}_y$. However, those of the LCP incident and RCP reflected waves are expressed as $\hat{e}_-^{\mathrm{i}} = \hat{e}_+^{\mathrm{r}} = \hat{e}_x - \mathrm{j}\hat{e}_y$. Thus, the reflection matrix $\boldsymbol{R}_{\text{cir}}$ for CP wave can be derived as follows:

$$\begin{aligned} \begin{pmatrix} E_+^{\mathrm{r}} \\ E_-^{\mathrm{r}} \end{pmatrix} &= \begin{pmatrix} 1 & -\mathrm{j} \\ 1 & \mathrm{j} \end{pmatrix} \begin{pmatrix} E_x^{\mathrm{r}} \\ E_y^{\mathrm{r}} \end{pmatrix} = \begin{pmatrix} 1 & -\mathrm{j} \\ 1 & \mathrm{j} \end{pmatrix} \begin{pmatrix} r_{uu}\cos^2\psi + r_{vv}\sin^2\psi & (r_{uu} - r_{vv})\cos\psi\sin\psi \\ (r_{uu} - r_{vv})\cos\psi\sin\psi & r_{uu}\sin^2\psi + r_{vv}\cos^2\psi \end{pmatrix} \begin{pmatrix} E_x^{\mathrm{i}} \\ E_y^{\mathrm{i}} \end{pmatrix} \\ &= \begin{pmatrix} 1 & -\mathrm{j} \\ 1 & \mathrm{j} \end{pmatrix} \begin{pmatrix} r_{uu}\cos^2\psi + r_{vv}\sin^2\psi & (r_{uu} - r_{vv})\cos\psi\sin\psi \\ (r_{uu} - r_{vv})\cos\psi\sin\psi & r_{uu}\sin^2\psi + r_{vv}\cos^2\psi \end{pmatrix} \begin{pmatrix} 1 & \mathrm{j} \\ 1 & -\mathrm{j} \end{pmatrix}^{-1} \begin{pmatrix} E_+^{\mathrm{i}} \\ E_-^{\mathrm{i}} \end{pmatrix}, \end{aligned} \tag{6}$$

$$\boldsymbol{R}_{\rm cir} = \begin{pmatrix} r_{++} & r_{-+} \\ r_{+-} & r_{--} \end{pmatrix} = \begin{pmatrix} 1 & -\mathrm{j} \\ 1 & \mathrm{j} \end{pmatrix} \begin{pmatrix} r_{uu}\cos^2\psi + r_{vv}\sin^2\psi & (r_{uu}-r_{vv})\cos\psi\sin\psi \\ (r_{uu}-r_{vv})\cos\psi\sin\psi & r_{uu}\sin^2\psi + r_{vv}\cos^2\psi \end{pmatrix} \begin{pmatrix} 1 & \mathrm{j} \\ 1 & -\mathrm{j} \end{pmatrix}^{-1}$$
$$= \frac{1}{2}\begin{pmatrix} (r_{uu}-r_{vv})\mathrm{e}^{+\mathrm{j}2\psi} & r_{uu}+r_{vv} \\ r_{uu}+r_{vv} & (r_{uu}-r_{vv})\mathrm{e}^{-\mathrm{j}2\psi} \end{pmatrix} = \frac{1}{2}r_{uu}\begin{pmatrix} \left(1-\mathrm{e}^{-\mathrm{j}\Delta\varphi_{uv}}\right)\mathrm{e}^{+\mathrm{j}2\psi} & 1+\mathrm{e}^{-\mathrm{j}\Delta\varphi_{uv}} \\ 1+\mathrm{e}^{-\mathrm{j}\Delta\varphi_{uv}} & \left(1-\mathrm{e}^{-\mathrm{j}\Delta\varphi_{uv}}\right)\mathrm{e}^{-\mathrm{j}2\psi} \end{pmatrix}. \tag{7}$$

Equation (7) illustrates that when the metallic patch in the unit cell of the PCM is rotated by an angle ψ in an anticlockwise direction, the PB phases generated in r_{++} and r_{--} will be $+2\psi$ and -2ψ, respectively. However, the phase of r_{+-} and r_{-+} will not be altered. Therefore, to design a reflective coding metasurface using PB phase, it must be based on an appropriate PCM, which can make the magnitude of r_{++} and r_{--} close to 1.0. Moreover, according to Eq. (7), the magnitudes of r_{++}, r_{--} and r_{+-}, r_{-+} can be expressed as

$$\begin{aligned} |r_{++}| = |r_{--}| &= \frac{1}{2}|r_{uu}|\left|1-\mathrm{e}^{-\mathrm{j}\Delta\varphi_{uv}}\right|\left|\mathrm{e}^{\pm\mathrm{j}2\psi}\right| \\ &= \sqrt{(1-\cos\Delta\varphi_{uv})/2}, \\ |r_{-+}| = |r_{+-}| &= \frac{1}{2}|r_{uu}|\left|1+\mathrm{e}^{-\mathrm{j}\Delta\varphi_{uv}}\right| \\ &= \sqrt{(1+\cos\Delta\varphi_{uv})/2}. \end{aligned} \tag{8}$$

Equation (8) indicates that the polarization conversion performance of the PCM can be determined by the phase difference $\Delta\varphi_{uv}$ between r_{uu} andr_{vv}. When the phase difference $|\Delta\varphi_{uv}|$ is close to 180°, the magnitudes of r_{++} and r_{--} will be close to 1.0, and the anticipated CP-maintaining reflection can be realized.

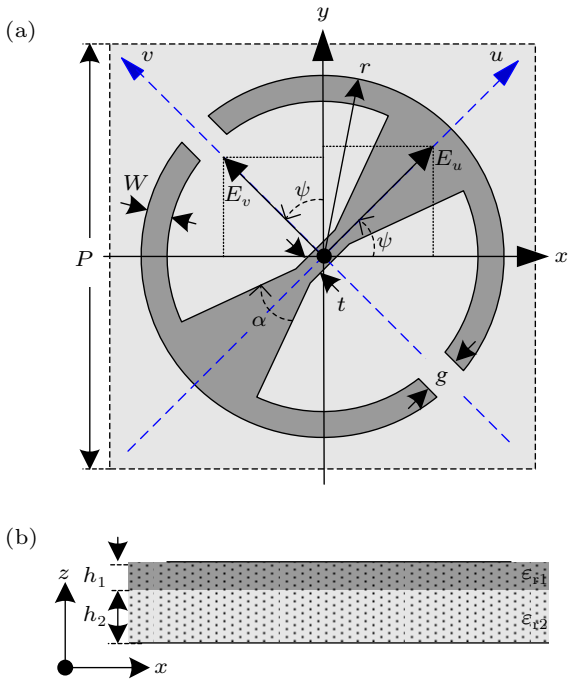


Fig. 1. Unit cell structure of the proposed PCM: (a) top view, (b) side view.

In order to analyze the performance of the proposed PCM, we have carried out a series of numerical simulations using CST Microwave Studio. First, it has been simulated under u- and v-polarized incidences. The simulated results, shown in Fig. 2(a), indicate that the phase difference $\Delta\varphi_{uv}$ of the PCM is close to 180° in the ultra-wide frequency range from 10 GHz to 43 GHz. In addition, according to the phase differences $\Delta\varphi_{xy}$ in Fig. 2(a), the magnitudes of r_{++} and r_{-+} have been calculated using Eq. (8). The calculated results, as shown in Fig. 2(b), indicate that the magnitude of r_{++} is approximately 0 dB, however, that of r_{-+} is kept less than −10 dB in the ultra-wide frequency band of 9.8 GHz–43.3 GHz, which shows that the anticipated CP-maintaining reflection will be realized in the ultra-wide band with a relative bandwidth of 126.2%. Furthermore, in order to verify the calculated results, the metasurface has been simulated under RCP incidence. In Fig. 2(b), it is shown that the calculated and simulated results are in good agreement with each other.

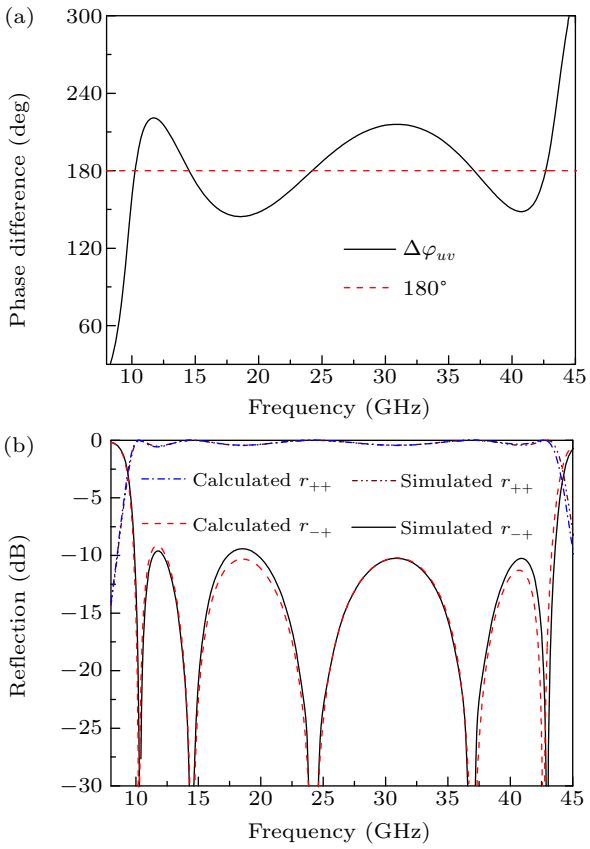


Fig. 2. Simulated results of the proposed PCM: (a) phase difference between r_{uu} and r_{vv}, (b) magnitude of r_{++} and r_{-+}.

Moreover, to verify that PB phase will be generated in the co-polarization reflection coefficients r_{++} and r_{--} by rotating the metallic patch in the unit cell of the proposed PCM, the

PCM has been repeatedly simulated under RCP and LCP incidences when the rotation angle ψ of the metallic patches in its unit cells was gradually increased from 0° to 157.5° with a 22.5° step width. The simulated results, shown in Figs. 3(a) and 3(b), indicate that along with the increase of the rotation angle ψ, the phase of r_{++} keeps increasing gradually but the phase of r_{--} keeps decreasing gradually in the ultra-wide frequency range from 8 GHz to 44 GHz, and they are both altered by almost 45.0° each time, which verifies that when rotation angle ψ is increased by $\Delta\psi$, the PB phases generated in r_{++} and r_{--} will be $+2\Delta\psi$ and $-2\Delta\psi$, respectively.

According to the simulated results in Fig. 3, it is known that when rotation angle ψ of the metallic patches in the PCM is gradually increased from 0° to 157.5° with a 22.5° step width, the PCM can always be used as coding elements of the coding metasurface. Based on the relative reflection phases of the PCM under RCP incidence, the code of the PCM at different states is listed in Table 1. It is shown that the PCM can be used to design 1-, 2-, and 3-bit coding metasurfaces. In this work, to design a 2-bit coding metasurface, the four coding elements, whose codes are "00", "01", "10", and "11", respectively, can be chosen as the PCM at the four states, wherein the rotation angle ψ of the metallic patches are 0°, 45°, 90°, and 135°, respectively.

Table 1. The relationship between the PCM at different states and 1-, 2-, and 3-bit coding metasurfaces.

Multi-bit	Rotation angle							
	$\psi = 0°$	$\psi = 22.5°$	$\psi = 45.0°$	$\psi = 67.5°$	$\psi = 90.0°$	$\psi = 112.5°$	$\psi = 135.0°$	$\psi = 157.5°$
Shape								
Reflection phase	0°	45.0°	90.0°	135.0°	180.0°	225.0°	270.0°	315.0°
1-bit	0				1			
2-bit	00		01		10		11	
3-bit	000	001	010	011	100	101	110	111

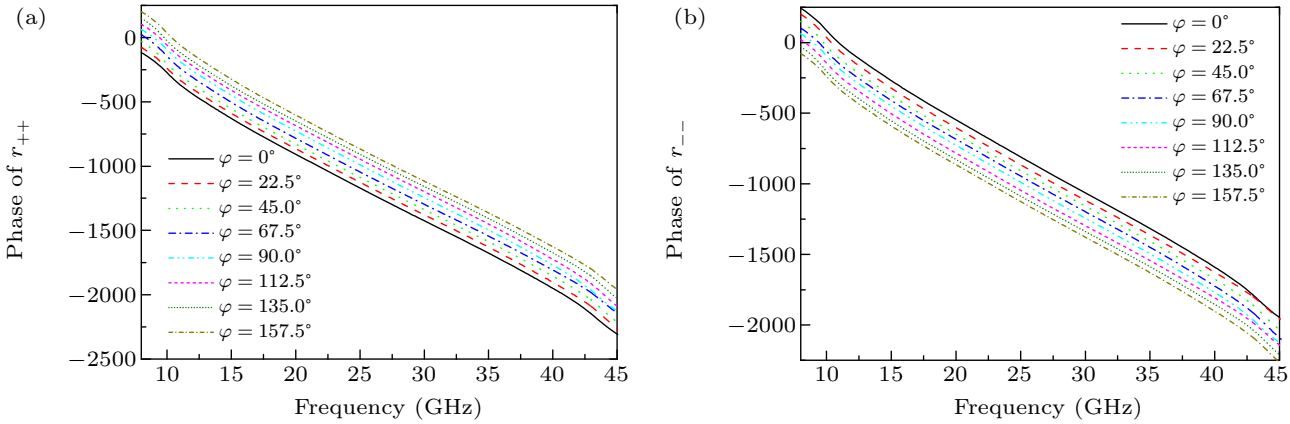


Fig. 3. Simulated results of the proposed PCM when the metallic patches in its unit cells are with different rotation angles ψ: (a) phase of r_{++}, (b) phase of r_{--}.

3. Design and analysis of the 2-bit coding metasurface

After the four coding elements were constructed, a 2-bit coding metasurface was proposed according to an appropriate coding sequence obtained by repeated simulations. The proposed 2-bit coding metasurface, shown in Fig. 4, consists of 6×6 coding elements, and each coding element is composed of 5×5 sub-unit cells. For the 2-bit coding metasurface, the reflection amplitudes in different elements are basically the same, but the reflection phases are different. The reflection phase difference between "00" and "10", together with that between "01" and "11", will be close to 180°. Thus, the anticipated RCS reduction can be realized due to the phase cancelation because these elements are arrayed according to an appropriate coding sequence.

To show the RCS reduction performance of our design, the 2-bit coding metasurface, together with a pure metallic plate of the same size, has been simulated under RCP, LCP, *x*-polarized (XP) and *y*-polarized (YP) normal incidences successively. The obtained simulated results, the mono-static

RCSs of the coding metasurface and the metallic plate, are shown in Fig. 5(a), in which it is shown that the monostatic RCS of the coding surface is almost the same under different polarization incidences, and the RCS is significantly reduced compared with that of the metallic plate. In addition, in Fig. 5(b), it is shown that under all incidences, the RCS reduction of the coding metasurface relative to the metal plate is kept larger than 10 dB from 9.8 GHz to 42.6 GHz except for 11.8 GHz to 12.6 GHz wherein RCS reduction is more than 8.4 dB, and the relative bandwidth reaches 125.2%. Moreover, the maximum RCS reduction under RCP, LCP, XP and YP normal incidence reaches 35.8 dB, 39.2 dB, 35.9 dB, and 39.7 dB, respectively, at 38.6 GHz. These simulated results indicate that the coding surface has the obvious advantages of wideband and polarization-insensitivity, it can realize ultra-wideband RCS reduction under arbitrary polarization incidences.

Table 2. Comparison of this work with previous works.

Ref.	σ_R (dB)	OFB (GHz)	FBW (%)	RBW
[14]	10	8.01–22.76	95.8	2.84
[15]	10	5.6–17.7	103.8	3.16
[16]	10	17–42	84.7	2.47
[17]	10	15–35	80	2.33
[18]	9	8.6–22.5	89.4	2.62
[19]	10	7.8–23.2	102.7	2.97
[22]	10	6.94–9.23	28.3	1.33
[25]	10	12.2–23.4	62.9	1.92
[26]	10	8.2–17.4	71.9	2.12
[29]	10	15–40	91	2.67
[30]	10	7.2–17.2	82	2.39
This work	10	9.8–42.6	125.2	4.35

σ_R: RCS reduction8.7
OFB: Operating frequency band
FBW: Fraction bandwidth (FBW $= (f_H - f_L)/f_C, f_C = (f_H + f_L)/2$)
RBW: Ratio bandwith (RBW $= f_H/f_L$)

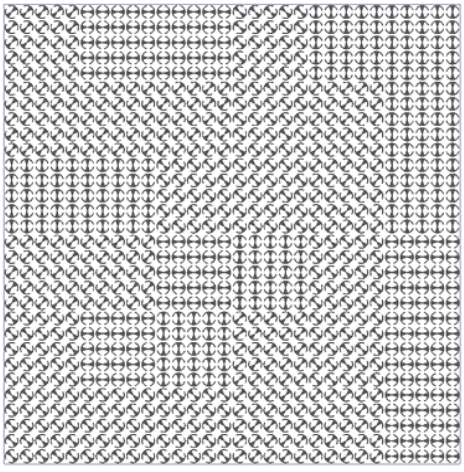


Fig. 4. Schematic diagrams of the proposed 2-bit coding metasurface.

Furthermore, to show far-field scattering characteristics of the 2-dit coding metasurface, the far-field scattering patterns of the coding metasurface and the metallic plate of the same size under LCP, RCP, XP and YP normal incidences were obtained at 10.0 GHz, 25.0 GHz, and 40.0 GHz through far-field simulation. The simulated results, shown in Fig. 6, indicate that compared with the strong specular reflection of the metal plate, the scattering field of the coding metasurface is diffused to all directions of the space in the specular reflection region. In addition, the far-field scattering characteristics of the coding metasurface are basically the same under LCP, RCP, XP and YP normal incidences, the bistatic RCS of the coding metasurface in most directions is reduced under different polarization incidences.

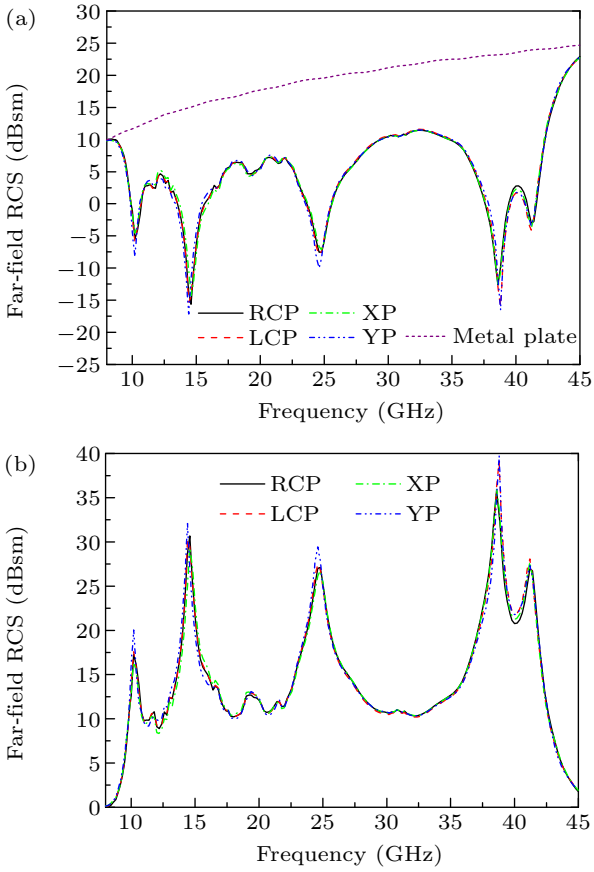
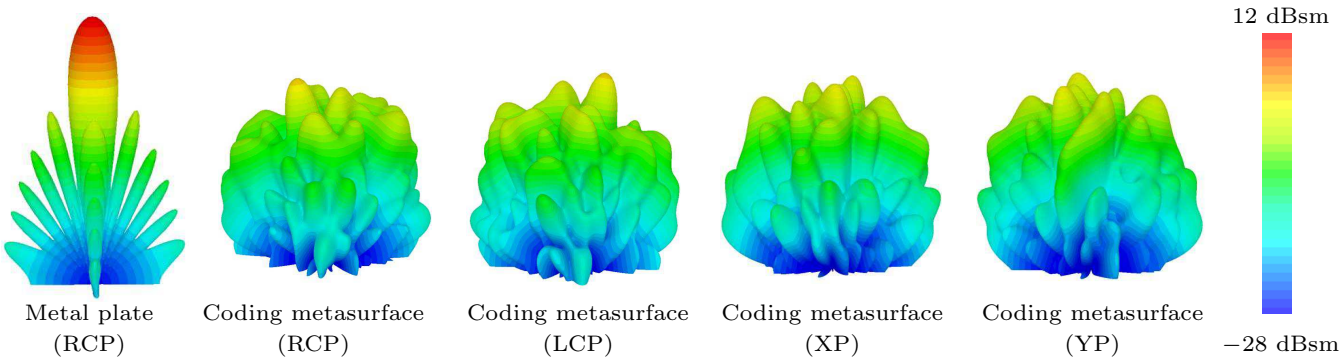
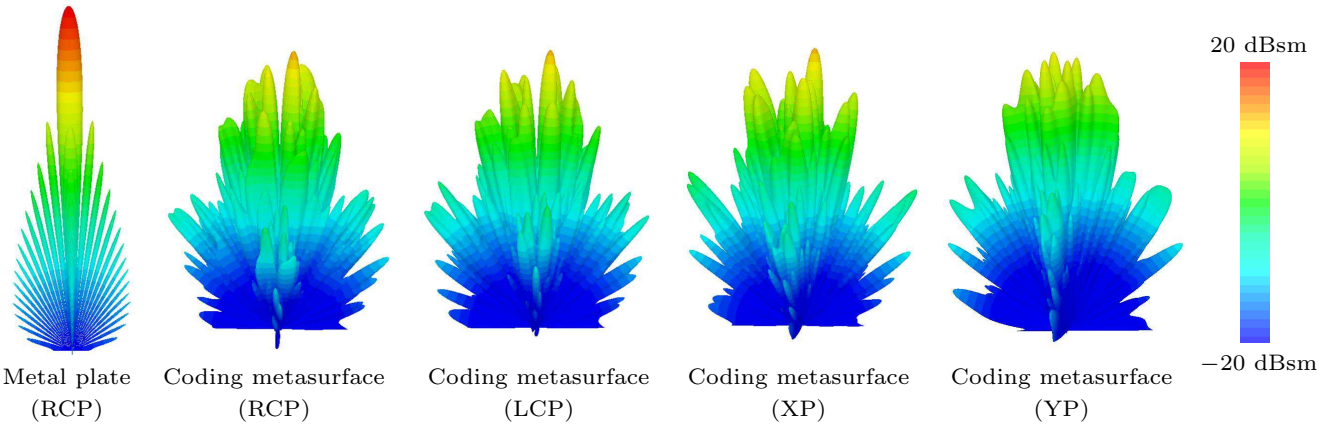


Fig. 5. Simulated results of the coding metasurface and the metallic plate: (a) monostatic RCS, (b) RCS reduction of the coding metasurface.

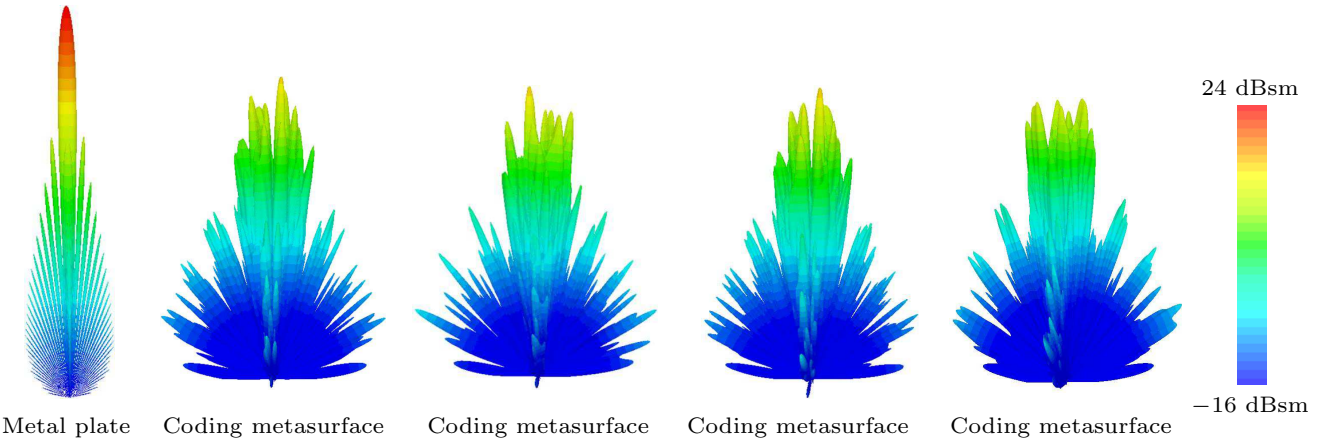
Finally, to experimentally verify the performance of the 2-bit coding metasurface, one laboratory sample has been fabricated using standard print circuit board (PCB) technique, which is shown in Fig. 7(a). The laboratory sample has been measured by the free space method. In addition, a metal plate of the same size has been measured in the same way as a reference. The measurement has been carried out under RCP, LCP, XP and YP normal incidences successively. The measured results are shown in Figs. 7(b) and 7(c). It is shown that the measured results under RCP and LP incidences are almost the same. In addition, the measurement results are in reasonable agreement with the simulated results, although there is a slight deviation caused by fabrication and measurement errors.



(a) 10.0 GHz



(b) 25.0 GHz



(c) 40.0 GHz

Fig. 6. Simulated 3D far-field scattering patterns of the proposed coding metasurface and the metal plate under different incidences at (a) 10.0 GHz, (b) 25.0 GHz, and (c) 40.0 GHz.

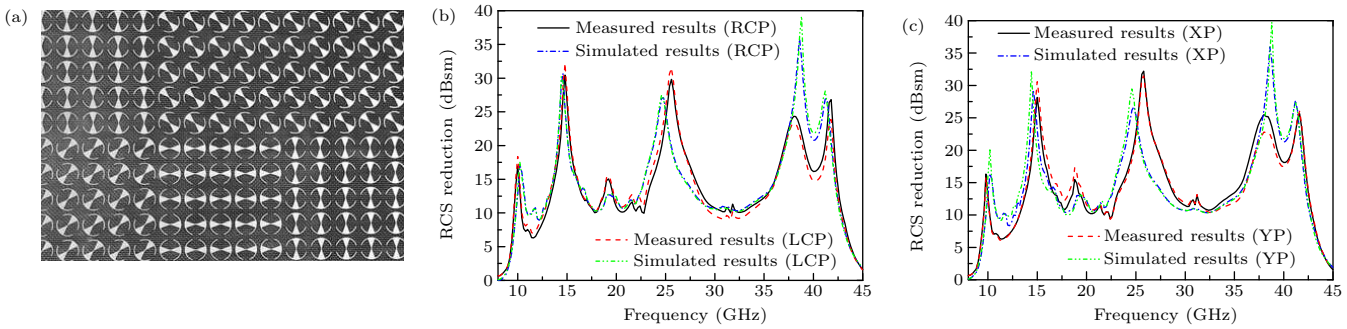


Fig. 7. Photographs of the experimental sample (a) and comparison of simulated and measured RCS reduction under RCP, LCP incidences (b) and XP, YP incidences (c).

4. Conclusion

In this paper, an ultra-wideband 2-bit PB coding metasurface was proposed based on an ultra-wideband PCM. The simulated results show that the RCS of the coding metasurface under arbitrary polarization incidences can be reduced by more than 10 dB RCS relative to a metallic plate of the same size in the frequency band from 9.8 GHz to 42.6 GHz except for 11.8 GHz to 12.6 GHz, and the relative bandwidth can be up to 125.2%. In addition, the coding metasurface has been successfully fabricated and measured, and there is a reasonable agreement between the simulated and measured results. Table 2 lists a comparison of the proposed coding metasurface with previous works. It is indicated that the coding metasurface has a significant advantage in the bandwidth expansion of RCS reduction. Moreover, the coding metasurface is polarization insensitive, so it has great application value in radar stealth technology application.

Acknowledgments

Project supported by the National Natural Science Foundation of China (Grant No. 62072378), the Natural Science Foundation of Shaanxi Province, China (Grant No. 2019JM-077), and the Xi'an Science and Technology Plan Project, China (Grant No. GXYD20.4).

References

[1] Ishii Y, Masaki T and Michishita N 2017 *IEICE Communications Express* **1** 1
[2] Wang M, Weng B and Zhao J 2017 *Appl. Phys. A* **123** 434
[3] Wang Y, Zhu D Y and Cui Z J 2020 *IEEE Transactions on Terahertz Science and Technology* **10** 599
[4] Xu H X, Wang G M, Qi M Q, *et al.* 2012 *Phys. Rev. B* **86** 205104
[5] Zhao M M, Fu S F, Zhou S, *et al.* 2020 *Chin. Phys. B* **29** 054210
[6] Ma E, Alvarez Y and Las-Heras F 2011 *Progress In Electromagnetics Research* **107** 147
[7] Modi A Y, Balanis C A and Birtcher C R 2017 *IEEE Trans. Antennas Propag.* **65** 5406
[8] Cong L, Cao X Y, Song T and Gao J 2018 *Chin. Phys. B* **27** 114101
[9] Zaker R and Sadeghzadeh A 2018 *IET Microwaves Antennas & Propagation* **12** 1601
[10] Ameri E, Esmaeli S H and Sedighy S H 2018 *J. Phys. D: Appl. Phys.* **51** 285304
[11] Sang D, Chen Q and Ding L 2019 *IEEE Trans. Antennas Propag.* **67** 2604
[12] Cui T J, Qi M Q, Wan X, Zhao J and Cheng Q 2014 *Light Sci. Appl.* **3** e218
[13] Liu X, Gao J, Xu L, Cao X, Zhao Y and Li S A 2016 *IEEE Antennas Wirel. Propag. Lett.* **16** 724
[14] Hui Z, Yao L, Su J, *et al.* 2016 *Electronics Letters* **53** 187
[15] Jia Y, Liu Y, Guo Y J, Li K and Gong S 2017 *IEEE Trans. Antennas Propag.* **65** 3291
[16] Sun H, Gu C, Chen X, *et al.* 2017 *Sci. Rep.* **7** 40782
[17] Hao H, Du S and Zhang T 2019 *Progress In Electromagnetics Research M* **81** 97
[18] Ali L, Li Q, Ali K T, Yi J and Chen X 2019 *Materials* **12** 2708
[19] Yuan F, Xu H X and Jia X Q 2020 *IEEE Trans. Antennas Propag.* **68** 2463
[20] Liang L, Wei M, Yan X, *et al.* 2016 *Sci. Rep.* **6** 39252
[21] Qi Y, Zhang B, Liu C and Deng X 2020 *IEEE Access* **8** 116675
[22] Han X, Xu H, Chang Y and Lin M 2020 *IEEE Access* **8** 162313
[23] Zhou C and Li J S 2020 *Chin. Phys. B* **29** 078706
[24] Qi Y, Zhang B, Ding J and Zhang T 2021 *Chin. Phys. B* **30** 024211
[25] Yuan F, Wang G M, Xu H X, Cai T and Zou X J 2017 *IEEE Antennas Wireless Propag. Lett.* **16** 3188
[26] Zhuang Y Q, Wang G M and Xu H X 2017 *Chin. Phys. B* **26** 054101
[27] Xu H X, *et al.* 2018 *ACS Photon.* **5** 1691
[28] Li S H and Li J S 2019 *Chin. Phys. B* **28** 094210
[29] Saifullah Y, Waqas A B, Yang G, Zhang F and Xu F 2019 *IEEE Access* **7** 122378
[30] Wang C, Xu H, Wang Y, Zhu S, Wang C and Mao R 2020 *J. Phys. D: Appl. Phys.* **53** 365001